2024 IEEE International Conference on Robotics and Automation (ICRA 2024)
May 13-17, 2024. Yokohama, Japan

Analysis and Validation of Stiffness and Payload of Nematode-Inspired Cable Routing Method for Cable Driven Redundant Manipulator

Hoyoung Kim, Jungwon Yoon*, *Member, IEEE*

***Abstract*— The cable-driven redundant manipulator (CDRM) has significant potential for applications in narrow and hazardous spaces. However, traditional CDRMs have limited stiffness and load capacity due to their cable routing method. To address these limitations, several scholars have proposed new mechanisms and control strategies. Nevertheless, the cable routing method has not changed, and CDRMs continue to suffer from their limitations. Recently, a nematode-inspired cable routing method was proposed; however, stiffness calculations, derivation of inverse kinematics, and validation of stiffness and load capacity were incomplete. In this paper, we calculate the analytic equivalent stiffness of the nematode-inspired cable routing method and compare it with other cable routing methods. Additionally, we derived and simulate the kinematics and an effective inverse kinematics algorithm. Finally, we validate the stiffness and load capacity using a developed prototype.**

I. Introduction

In recent years, there has been an increasing demand for manipulators capable of operating in narrow or hazardous spaces [1]. These applications include tasks such as pipe inspection [2], nuclear plant maintenance [3], space applications [4], aircraft assembly [5], life search and rescue missions [6], among others. A manipulator developed for use in narrow and hazardous spaces should possess various capabilities, including obstacle avoidance, singularity reduction, a large and extensive reachable workspace, and the ability to ensure the necessary load capacity for both the end-effector tool and external load handling [7].

The cable-driven redundant manipulator (CDRM) has gained attention for applications in narrow and hazardous spaces due to its high dexterity and small body diameter. One of the most well-known examples of the traditional CDRMs is the snake-arm robot developed by OC Robotics [8]. The joint structure of the snake-arm robot consists of a large number of universal joints, with three cables used for driving each universal joint [7-8]. However, the traditional CDRMs exhibit limitations in terms of the joint structure and the cable routing methods. The limited range of motion of the joint structure, resulting from the use of universal joints, necessitating a higher number of joints and cables to achieve greater dexterity. Moreover, the limited stiffness and load capacity of the cable routing method can lead to decreased system performance. To address these limitations, various studies have proposed new control schemes or mechanisms. Xu, Wenfu, et al [1], analyzed the kinematics and dynamics of the traditional CDRMs to improve control performance. The study derived the kinematics and dynamics of traditional CDRMs, applying dynamic control strategies to enhance control accuracy. Huang, Yifan, et al [9], utilized the quaternion joint to increase the maximum joint angle of CDRMs. This quaternion joint [10] was developed to actuate a robot wrist driven by cables, providing two degrees of freedom and a large bending angle of about 90 degrees. It enables CDRMs to have a larger workspace and higher dexterity while using fewer motors than the traditional CDRMs. Liu, Tianliang, et al [11], applied the active-passive-linkage segment mechanisms to the traditional CDRMs to augment stiffness and load capacity. The proposed mechanism can enhance stiffness and load capacity while maintaining manipulator dexterity and end-effector accuracy. Yang, Taiwei, et al [12], proposed a new CDRM that combines the advantages of the quaternion joint and segmented coupled linkages mechanism. This design provides a large and extensive reachable workspace through quaternion joints with improved stiffness and load capacity via segmented coupled linkages mechanisms.

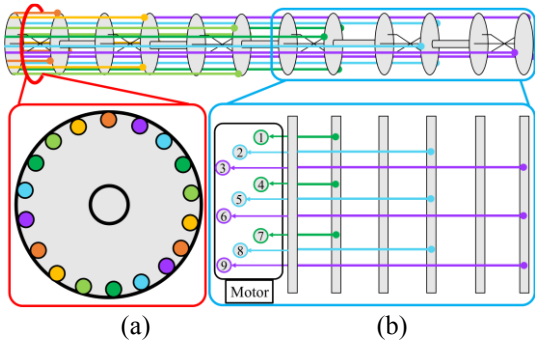

Fig. 1. Schematic of the traditional cable routing method in the (a) cross-sectional plane, (b) head-tail plane.

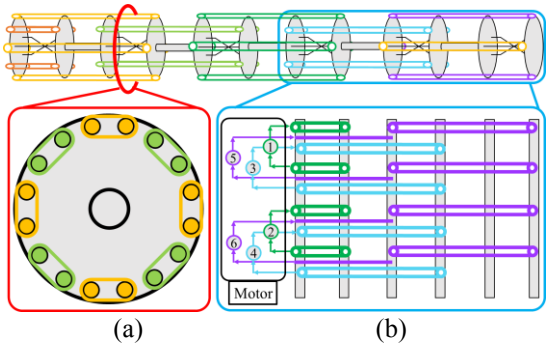

Fig. 2. Schematic of the nematode-inspired cable routing method in the (a) cross-sectional plane, (b) head-tail plane.

Hoyoung Kim is with Gwangju Institute of Science and Technology(GIST), Gwangju, Republic of Korea (Tel: +82-62-715-5351, email: hoyoungkim@gm.gist.ac.kr) Jungwon Yoon, is with Gwangju Institute of Science and Technology(GIST), Gwangju, Republic of Korea (Tel: +82-62-715-5332, email: jyoon@gist.ac.kr)

However, as shown in Fig. 1, the cable routing method used in these studies remains the same as the cable routing method of traditional CDRMs. Therefore, they continue to suffer from limitations in terms of stiffness and load capacity. Hoyoung Kim, et al [13], have proposed a study on a new cable routing method inspired by nematodes. The nematode-inspired cable routing method is based on the muscle structure of the nematodes, which provides dexterity in movement and muscle force for CDRMs as shown in Fig. 2. To mimic the muscle structure, an alternately arranged moving pulley structure is used to enhance the stiffness and load capacity, while quaternion joints are used for each joint to provide large joint angles. In this study, the authors derived an equivalent stiffness equation using a simplified stiffness model of CDRMs based on the serial and parallel springs model along with the kinematics equation of the prototype. Then, kinematics and stiffness of the developed prototype were validated by experiments. Nevertheless, it is essential to derive an analytic equation for stiffness estimation. Additionally, the stiffness and load capacity of the prototype were not completely validated.

In this paper, we calculate an analytic equivalent stiffness and compare it with the equivalent stiffness of each cable routing method. Moreover, an inverse kinematics algorithm based on the Forward and Backward Reaching Inverse Kinematics (FABRIK) algorithm was derived and simulated. Finally, we validate not only the dexterity of the prototype but also its stiffness and load capacity.

The remainder of this paper is structured as follows. In Section II, the basic concept of the nematode-inspired cable routing method is introduced. In Section III, the kinematics and inverse kinematics algorithms are derived and simulated. In section IV, equivalent stiffness is calculated and a comparison of the stiffness of each method is presented. In section V, developed prototype and the validation of the stiffness and load capacity are presented. Finally, in section VI, concludes this paper.

II. Basic Concept of the Cable Routing Method

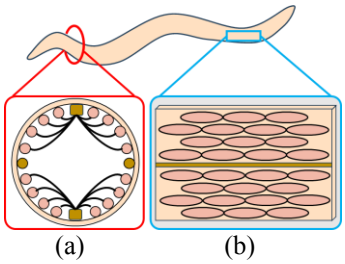

Fig. 3. The muscle structure of the nematodes in the (a) cross-sectional plane, (b) head-tail plane.

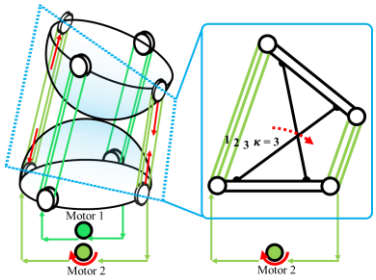

Fig. 4. Schematic of the quaternion joint driven by a moving pulley structure.

This section reviews the basic concept of the nematode-inspired cable routing method presented in [13]. The main concept of this system is divided into cable routing method and joint structure. The basic concept of the cable routing method can be explained using the muscle structure of nematodes. The nematode-inspired cable routing method mimics the muscle structure of nematodes, as shown in Fig. 3. In the cross-sectional plane of the nematodes, as shown in Fig. 3(a), the body wall muscles are arranged radially. On the other hand, in the head-tail plane of the nematodes, as shown in Fig. 3(b), the body wall muscles are arranged alternately [14]. From this muscle structure, nematode can have complex movement and muscle force for locomotion. To mimic this muscle structure, our cable routing method arranges the moving pulley structure to closely resemble it.

The basic concept of the joint structure can be explained using the Quaternion joint. The mechanism of the quaternion joints is based on the anti-parallelogram mechanism, which can approximate 2-DOF spherical rolling motion. This 2-DOF joint can be driven by two pairs of facing moving pulley structures, which have 90-degree offset between them, and each pairs can be driven by one motor. Fig. 4 shows the example of the quaternion joint with two pairs of facing moving pulley structures. In this figure, the cable winding number κ is 3, which means the number of cables wound on the moving pulley. The stiffness of the quaternion joint increases in proportion to the square of κ.

Based on these two basic concepts, we proposed a new cable routing method. Fig. 1 shows the schematic of the traditional cable routing method, while Fig. 2 shows the schematic of the nematode-inspired cable routing method. The traditional cable routing method arranges cables radially in the cross-sectional plane as shown in Fig. 1(a), while arranging them like a stair in the head-tail plane as shown in Fig. 1(b). In this case, the number of arranged cables gradually decreases towards the end. Additionally, another cable routing method suggested in [9] uses four cables for driving each joints. However, the cable arranging method is essentially the same as explained above. On the other hand, the nematode-inspired cable routing method arranges the moving structure radially in the cross-sectional plane as shown in Fig. 2(a), and alternately in the head-tail plane as shown in Fig. 2(b). In this case, the number of arranged moving pulleys does not decrease towards the end. This alternately arranged moving pulley structure can enhance the stiffness and load capacity of the CDRMs.

The stiffness of each cable routing method can be compared using the simplified stiffness model described in [13], which is based on the serial and parallel spring models.

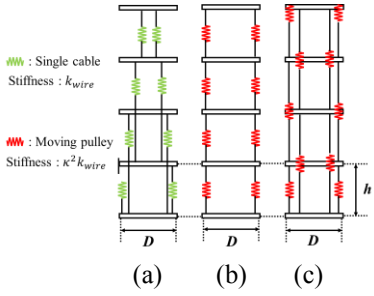

Fig. 5. Simplified stiffness model of (a) traditional, (b) serially arranged moving pulley, (c) nematode-inspired cable routing method

The simplified stiffness model of each cable routing method is shown in Fig. 5. The simplified stiffness of the traditional cable routing method (Fig. 5(a)) can be treated as a serial spring connection of the cable, and the serially arranged moving pulley cable routing method (Fig. 5(b)) can be treated as a serial spring connection of the moving pulley structure, while nematode-inspired cable routing method (Fig. 5(c)) can be treated as parallel spring connection of the moving pulley structure. The equivalent stiffness equation was derived in [13] with cable winding number is 3, as follows:

$$k_{Traditional} = \frac{12d}{25h} k_{wire} \tag{1}$$

$$k_{Nematode-inspired} = \frac{18d}{5h} k_{wire} \tag{2}$$

where D is the diameter of the joint frame, h is the height of between two joint frames, and k_{wire} is the cable stiffness. The amplification ratio between simplified stiffness of the traditional and nematode-inspired cable routing method was calculated by 7.5. Therefore, proposed method can increase the stiffness of the CDRMs. However, the amplification ratio between serially arranged moving pulley cable routing method and nematode-inspired cable routing method was not calculated in this study. Furthermore, the stiffness calculated by simplified model is far from the actual stiffness and insufficient to calculate the stiffness of entire CDRM. To calculate the equivalent stiffness of CDRM, the kinematics of CDRM was derived in section III, and the analytic equivalent stiffness model was derived in section IV.

III. Forward Kinematics & Inverse Kinematics

A. Forward Kinematics

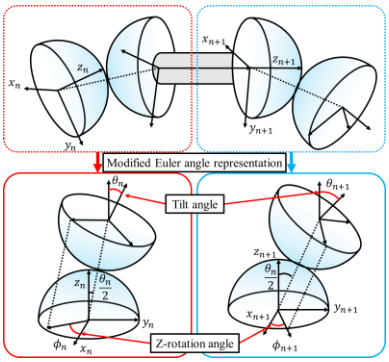

Fig. 6. Modified Euler angle representation of the joint angle of the single joint set.

To apply the alternately arranged moving pulley structure to the quaternion joint, two connected quaternion joints are regarded as a single joint set. As shown in Fig. 6, the joint angle of the single joint set is defined using the modified Euler angle representation [15]. ϕ represents the angle difference between the two frames of each quaternion joint, while θ represents the tilt angle of each quaternion joint. Using the angles ϕ and θ, we can derive the kinematics of the single joint set through a homogeneous transformation, as follows:

$$H_n = R_z(\phi_n) R_y\left(\frac{\theta_n}{2}\right) T_{z,h} R_y\left(\frac{\theta_n}{2}\right) R_z(-\phi_n) \tag{3}$$

$$H_{n+1} = R_z(\phi_{n+1}) R_y\left(\frac{\theta_{n+1}}{2}\right) T_{z,h} R_y\left(\frac{\theta_{n+1}}{2}\right) R_z(-\phi_{n+1}) \tag{4}$$

$$A = H_n \times H_{n+1} = \begin{bmatrix} R_n^{n+1} & o_n^{n+1} \\ 0 & 1 \end{bmatrix} \tag{5}$$

where H is the homogeneous transformation matrix between the two frames of each quaternion joint, R is the rotational transformation matrix, and T is the translational transformation matrix. h represents the height of each quaternion joint. Matrix A is obtained by multiplying equations (3) and (4). It represents the homogeneous transformation matrix of the single joint set. From the obtained homogeneous matrix, we can represent the relationship between the joint angle and the end-effector position of the single joint set using the analytical Jacobian matrix as follows:

$$\dot{X} = \begin{bmatrix} \frac{\partial R_n^{n+1}}{\partial \Theta} \\ \frac{\partial o_n^{n+1}}{\partial \Theta} \end{bmatrix} \dot{\Theta} = J_X \dot{\Theta} \tag{6}$$

where $\dot{X}$ is the velocity of the end-effector, $\dot{\Theta}$ is the change in the joint angle, and J_X is the analytical Jacobian matrix of the end-effector for single joint set. To create the alternately arranged moving pulley structure, the cable routing method is divided into two types, based on the offset between them.

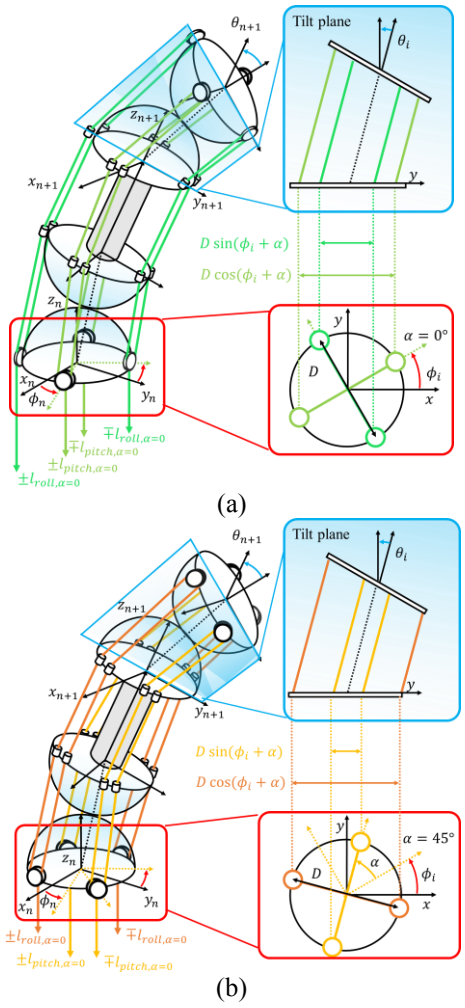

Fig. 7. Schematic of (a) cable routing method with zero-degree offset, (b) cable routing method with 45-degree offset.

As shown in Fig. 7, a single joint set was utilized to alternately arrange moving pulley structures on the entire CDRM with a 45-degree offset between the two cable routing methods. The cable routing method, consist of two pairs of facing moving pulley structure arranged with a zero-degree offset as shown in Fig. 7(a), and a 45-degree offset as shown in Fig. 7(b). Each quaternion joint of the single joint set has 2-DOF motion, which include rolling and pitching motions. To drive this motion, the cable length change in one pair of moving pulleys should be the same, while the direction is opposite. Therefore, the cable length changes for each cable routing method can be represented as follows:

$$\begin{cases} \pm l_{roll} = \sum_{i=n}^{n+1} \kappa D \sin(\phi_i + \alpha) \sin\left(\frac{\theta_i}{2}\right) \\ \pm l_{pitch} = \sum_{i=n}^{n+1} \kappa D \cos(\phi_i + \alpha) \sin\left(\frac{\theta_i}{2}\right) \end{cases} \quad (7)$$

where l_{roll} is the driving cable length change for the rolling motion of the single joint set, while l_{pitch} is the driving cable length change for the pitching motion of the single joint set. κ is the cable winding number of the moving pulley structure, D is the diameter of the single joint set, and α is the offset angle of the cable routing method. From the obtained cable length change of the single joint set, the relationship between the cable length change and the joint angles can be presented by the Jacobian matrix, as follows:

$$\dot{L} = \begin{bmatrix} \frac{\partial \pm l_{roll}}{\partial \Theta} \\ \frac{\partial \pm l_{pitch}}{\partial \Theta} \end{bmatrix} \dot{\Theta} = J_C \dot{\Theta} \quad (8)$$

where the $\dot{L}$ is the change in the cable length, $\dot{\Theta}$ is the change in joint angle, and J_C is the cable length Jacobian matrix of the cable routing method applied to the single joint set.

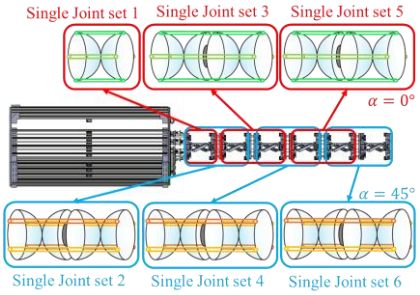

Fig. 8. Schematic of the prototype configuration($\boldsymbol{\alpha}$ is the offset angle between the cable routing method)

Through the forward kinematics of the single joint set and the cable routing method, we can derive the forward kinematics of the entire CDRM. Fig. 8 shows the schematic configuration of the prototype used in this study. As shown in Fig. 8, the prototype is composed of six single joint sets and two cable routing methods. By this structure, the nematode-inspired cable routing method introduced in Fig. 2 and Fig. 5(c) was implemented. To ensure that the prototype is fully actuated, the first joint set is composed of one quaternion joint and a zero-degree offset cable routing method is applied. From the second single joint set to the sixth single joint set, 45-degreess offset cable routing method and zero-degree offset cable routing methods are alternately arranged from the base to the end effector. The forward kinematics relationship between the joint angle and the end effector of the prototype is as follows:

$$\dot{X}_e = J_{X_e} \dot{\Theta}_e \quad (9)$$

where $\dot{X}_e$ is the change in end effector position of the entire prototype, $\dot{\Theta}_e$ is the change in the joint angle of the entire prototype, J_{X_e} is the position Jacobian matrix of the entire prototype. Next, the forward kinematics relationship between the cable length and the joint angle of the prototype is as follows:

$$\dot{L}_e = J_{C_e} \dot{\Theta}_e \quad (10)$$

where $\dot{L}_e$ is the change in cable length of the entire prototype, $\dot{\Theta}_e$ is the change in joint angle of the entire prototype, J_{C_e} is the cable Jacobian matrix of the entire prototype. These two Jacobian matrices can be used to represent the relationship between the change in cable length and the change in end effector position change.

B. Inverse Kinematics

Recently, an effective inverse kinematics algorithm for CDRMs composed of quaternion joints; was proposed in [9]. This algorithm is based on the Forward and Backward Reaching Inverse Kinematics (FABRIK) algorithm, which is an efficient two-stage iteration algorithm, with the addition of angle limit avoidance for the joints. Using this algorithm, we can solve the inverse kinematics of our prototype. To verify the inverse kinematics algorithm, a trajectory planning simulation was conducted using Matlab®. The discretized desired circular trajectory is described in equation (11). All joints have 90-degree angle limit.

$$\begin{cases} P_E = [500\cos j\,, 50 + 500\sin(j)\,, 700]^T, j = 0{\sim}2\pi \\ \vec{O}_E = [0.6, 0, 0.8]^T \end{cases} \quad (11)$$

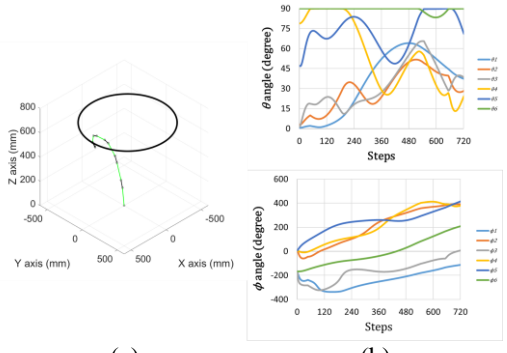

(a) (b)

Fig. 9. Simulation result of (a) circular trajectory and (b) angle change.

The simulation result for circular trajectory planning is shown in Fig. 9(a), and the angle change in trajectory planning is shown in Fig. 9(b). These results show that the inverse kinematics algorithm can successfully plan the desired path for the CDRM while avoiding angle limits.

IV. Equivalent Stiffness Calculation

The stiffness of the entire CDRMs can be calculated according to the principle of virtual work [4], [16]. In this

paper, we assume that the effects of friction and gravity effect are negligible. Therefore, the static model of the CDRMs is as follows:

$$F_{e_e}^T \delta X_e - F_{C_e}^T \delta L_e = 0 \quad (12)$$

where $F_{e_e}^T$ is the external force vector and $F_{C_e}^T$ is the cable driving force vector, X_e is the end effector position vector and L_e is the cable length vector. Substituting $\delta X_e = \frac{\partial X_e}{\partial \Theta_e} d\Theta_e$, and $\delta L_e = \frac{\partial L_e}{\partial \Theta_e} d\Theta_e$, into equation (12), we obtain:

$$F_{e_e}^T \frac{\partial X_e}{\partial \Theta_e} d\Theta_e - F_{C_e}^T \frac{\partial L_e}{\partial \Theta_e} d\Theta_e = 0. \quad (13)$$

Substituting $\frac{\partial X_e}{\partial \Theta_e} = J_{X_e}$ and $\frac{\partial L_e}{\partial \Theta_e} = J_{C_e}$ into equation (13) and taking the transpose of it, we have:

$$J_{X_e}^T F_{e_e} - J_{C_e}^T F_{C_e} = 0. \quad (14)$$

To obtain the equivalent stiffness, we need to derive the relationship between deformation and the change in the external force of the CDRMs. Differentiating equation (14), we get:

$$dJ_{X_e}^T F_{e_e} + J_{X_e}^T dF_{e_e} - dJ_{C_e}^T F_{C_e} - J_{C_e}^T dF_{C_e} = 0. \quad (15)$$

In this paper, we suppose external force and driving force are zero. Hence, equation (15) can be written as follows:

$$J_{X_e}^T dF_{e_e} = J_{C_e}^T dF_{C_e}. \quad (16)$$

Substituting $dF_{C_e} = \frac{\partial F_{C_e}}{\partial L_e} \frac{\partial L_e}{\partial \Theta_e} d\Theta_e$ into equation (16), we have:

$$J_{X_e}^T dF_{e_e} = J_{C_e}^T K_C J_{C_e} d\Theta_e \quad (17)$$

where $K_C = \frac{\partial F_{C_e}}{\partial L_e}$, which is the cable stiffness diagonal matrix. The matrix $J_{C_e}^T K_C J_{C_e}$ is a square matrix, and we can take its inverse on both sides of equation (17), resulting in:

$$d\Theta_e = (J_{C_e}^T K_C J_{C_e})^{-1} J_{X_e}^T dF_{e_e}. \quad (18)$$

Substituting equation (18) into $d\mathrm{X}_e = J_{X_e} d\Theta_e$, we have:

$$d\mathrm{X}_e = J_{X_e} (J_{C_e}^T K_C J_{C_e})^{-1} J_{X_e}^T dF_{e_e}. \quad (19)$$

Finally, the stiffness of the CDRMs can be defined by $K_{CDRM} = \frac{\partial F_{e_e}}{\partial \mathrm{X}_e}$. Taking the inverse of the square matrix $J_{X_e}(J_{C_e}^T K_C J_{C_e})^{-1} J_{X_e}^T$ on both sides of equation (19), we obtain:

$$K_{CDRM} = \left[J_{X_e} (J_{C_e}^T K_C J_{C_e})^{-1} J_{X_e}^T \right]^{-1} \quad (20)$$

Pseudo inverse calculations are not required during the derivation, allowing us to successfully calculate the stiffness matrix of the redundant.

With the obtained stiffness matrix, the stiffness of the CDRMs can be calculated by equation (21), which is the method presented in [4].

$$k_{CDRM} = \sqrt{k_x^2 + k_y^2 + k_z^2} \quad (21)$$

where k_{CDRM} is the stiffness of the CDRM, k_x, k_y, k_z are the stiffness of the CDRMs in x-axis, y-axis, z-axis.

The calculation parameter and results are listed in Table 1. In calculation, all joint tilt angle of the CDRM are 0.001° to avoid the singularity of the kinematics. In Table I, NCDRM is the stiffness of the nematode-inspired cable routing method, MCDRM is the stiffness of the serially arranged moving pulley cable routing method, and TCDRM is the stiffness of the traditional cable routing method.

Table I. Equivalent stiffness calculation result

Cable stiffness (N/mm)	0.5858			
Cable winding number, κ	3	4	5	6
NCDRM (10^9 N/mm)	3.75	7.09	11.56	16.95
MCDRM (10^9 N/mm)	2.06	3.93	6.35	9.34
TCDRM (10^9 N/mm)	0.24	0.24	0.24	0.24
NCDRM / MCDRM	1.8198	1.8057	1.8084	1.8147
NCDRM / TCDRM	15.4451	29.1920	47.3067	69.7919

NCDRM : Stiffness of the entire CDRM with nematode-inspired cable routing method
MCDRM : Stiffness of the entire CDRM with serially arranged moving pulley cable routing method
TCDRM : Stiffness of the entire CDRM with traditional cable routing method

As shown in the result, NCDRM is approximately 15 times larger than TCDRM and approximately 2 times larger than MCDRM when the cable winding number is 3. The amplification ratio between NCDRM and MCDRM not change considerably when the cable winding number is increased. However, the amplification ratio between NCDRM and TCDRM rapidly increases. Based on these findings, we can conclude that the structure of our proposed cable routing method can amplify the stiffness of the entire CDRM more effectively than using serially arranged moving pulley cable routing method. Additionally, the equivalent stiffness model can calculate analytic stiffness of entire CDRM, which was not achievable with simplified stiffness model in [13].

V. Experimental Validation

A. Prototype

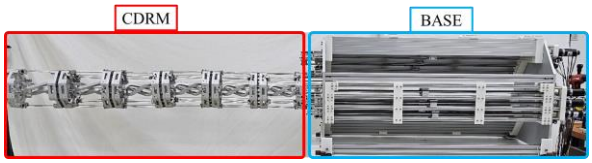

Fig. 10. Developed prototype

Table II. Prototype design parameter

Total length of CDRM (mm)	1160
Diameter of CDRM(mm)	150
Total degrees of freedom	12
Number of segments	6
Number of motors	12
Moving pulley winding number	3

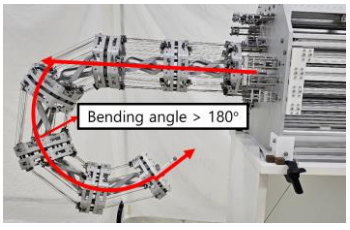

Fig. 111. Bending angle example of the prototype

Fig. 10 represents the developed prototype based on the joint structure and cable routing method introduced in Section II and III. The prototype's structure is constructed from aluminum, and a strand steel wire rope with a diameter of 0.81 mm and a breaking force of 585.8 N is used for the cable routing method. To drive the prototype, we are using 12 ball screws each controlled by a DC motor. To approximate the spherical rolling motion of the quaternion joint, we employ using the approximation method for a spherical rolling joint as introduced in [10]. The maximum approximation error for spherical rolling motion is 0.0890 mm; when h_0 = 5 mm, w_c =38 mm, h_c =125 mm. The design parameters of the prototype are listed in Table. II. The bending angle example of the prototype was larger than 180°, as shown in Fig. 11, which indirectly demonstrates the prototype has high dexterity.

B. Stiffness & Load capacity Experiment

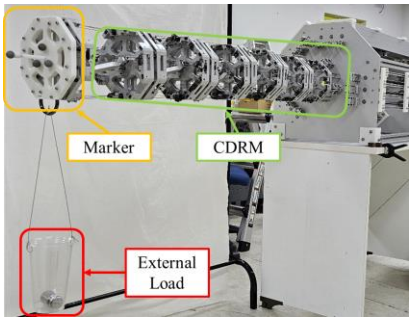

Fig. 122. Experimental setup for stiffness measurement

Table III. Stiffness measurement result

External Load (g)	400	800	1200	1600	2000
Maximum Displacement (mm)	1.6772	2.9917	4.3935	6.2340	7.9933
Stiffness (N/mm)	2.3396	2.6232	2.6794	2.5178	2.4545

Maximum stiffness (N/mm)	Minimum stiffness (N/mm)	Average stiffness (N/mm)
2.6794	2.3396	2.5229

Table IV. Stiffness and load capacity comparison

	Length (mm)	Stiffness (N/mm)	Load capacity (kg)
CDHM [1]	1500	-	2.5
S-CDRSM [4]	1680	0.25~0.35	1.5
CSRM [17]	1265	0.657	1.5
NCDRM	1160	2.5529	5.0

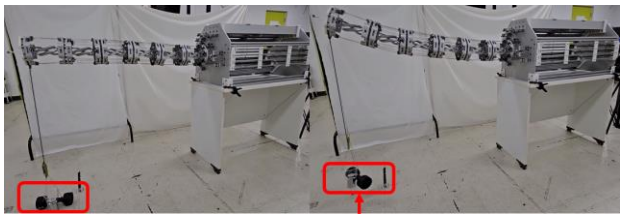

Fig. 133. Experiment for load capacity measurement of the prototype

To validate the stiffness of the prototype, we measured it by calculating the displacement caused by a given external load at the end effector. The prototype was driven by 12 DC motors with a nominal torque of 1 Nm and a maximum speed of 90 rpm. The displacement at the end effector was measured using a marker, as shown in Fig. 12. The measurements were conducted with external loads of up to 2 kg, and the resulting displacement were measured three times for each external load. Table III shows the measurement results of the experiment. In the results, the maximum stiffness was 2.6794 N/mm and the minimum stiffness was 2.3368 N/mm. The average stiffness was 2.5529 N/mm, with 0.1350 N/mm standard deviation. Because the analytic equivalent stiffness model assumed an ideal condition that neglecting friction, gravity effect and other considerations, the measured stiffness is lower than the simulated stiffness. Furthermore, a load capacity was measured using the developed prototype as shown in Fig. 13. The load capacity of the prototype, as indicated by NCDRM, was 5.0 kg, as shown in Table IV. Table IV presents the stiffness and load capacity of each CDRM in order to compare the performance of the prototype to that of other CDRMs. The stiffness of prototype was 4 to 10 times larger than that of other CDRMs and the load capacity of prototype was 2 to 3 times larger than that of other CDRMs, which demonstrating remarkable stiffness and load capacity performance. The stiffness amplification ratio was smaller than the calculated equivalent stiffness, because the calculated stiffness does not consider the gravitational effect of the CDRMs.

VI. Conclusion

In this paper, we have validated that our proposed method can enhance the stiffness and load capacity of the CDRM through equivalent stiffness calculations and experiments. Additionally, an inverse kinematics algorithm was derived and verified by simulation. Based on the calculation results, the equivalent stiffness of our cable routing method is approximately 15 times larger than the traditional method when the cable winding number is 3. The inverse kinematics algorithm was derived and verified through path planning simulation with Matlab®. In the experiments, we validated the stiffness of the prototype. The measured average stiffness of the developed prototype was 2.5229 N/mm, with 0.1350 N/mm standard deviation, which is 4 to 10 times larger than that of traditional CDRMs, and load capacity was 5 kg. Furthermore, the bending angle of the prototype was larger than 180°, which demonstrates high dexterity indirectly.

In future research, we will apply the inverse kinematics algorithm with feedback control strategies to conduct trajectory tracking experiment and reduce the delay effect to enhance control performance. Additionally, we will develop a path planning algorithm for obstacle avoidance and end effector tool control for practical application.

Acknowledgements

This work was supported by the Translational Research Center for Rehabilitation Robots (#NRCTR-EX23010), National Rehabilitation Center, Ministry of Health and Welfare, Korea and the Culture, Sports and Tourism R&D Program through the Korea Creative Content Agency grant funded by the Ministry of Culture, Sports and Tourism in 2023. (Project Name: Development of personalized exhibition viewing concierge service technology for the visually impaired, Project Number: RS-2023-00303777, Contribution Rate: 50%)

REFERENCES

[1] Xu, Wenfu, Tianliang Liu, and Yangmin Li. "Kinematics, dynamics, and control of a cable-driven hyper-redundant manipulator." IEEE/ASME Transactions on Mechatronics 23.4 (2018): 1693-1704.

[2] Luo, Mingrui, et al. "A Bioinspired Coiled Cable-Driven Manipulator: Mechatronic Design and Kinematics Planning With Multiconstraints." IEEE/ASME Transactions on Mechatronics (2023).

[3] Buckingham, Rob, and Andrew Graham. "Nuclear snake-arm robots." Industrial Robot: An International Journal 39.1 (2012): 6-11.

[4] Jianqing, P. E. N. G., et al. "Workspace, stiffness analysis and design optimization of coupled active-passive multilink cable-driven space robots for on-orbit services." Chinese Journal of Aeronautics 36.2 (2023): 402-416.

[5] Buckingham, Rob, et al. Snake-arm robots: a new approach to aircraft assembly. No. 2007-01-3870. SAE Technical Paper, 2007.

[6] Wolf, Alon, et al. "A mobile hyper redundant mechanism for search and rescue tasks." Proceedings 2003 IEEE/RSJ International Conference on Intelligent Robots and Systems (IROS 2003) (Cat. No. 03CH37453). Vol. 3. IEEE, 2003.

[7] Bogue, Robert. "Snake robots: A review of research, products and applications." Industrial Robot: An International Journal 41.3 (2014): 253-258.

[8] Buckingham, R. O., and A. C. Graham. "Dexterous manipulators for nuclear inspection and maintenance—Case study." 2010 1st International Conference on Applied Robotics for the Power Industry. IEEE, 2010.

[9] Huang, Yifan, et al. "Sensing design, trajectory planning, and motion control of a cable-driven redundant manipulator composed of quaternion joints." Journal of Mechanisms and Robotics 15.5 (2023): 055001.

[10] Kim, Yong-Jae, Jong-In Kim, and Wooseok Jang. "Quaternion joint: Dexterous 3-DOF joint representing quaternion motion for high-speed safe interaction." 2018 IEEE/RSJ International Conference on Intelligent Robots and Systems (IROS). IEEE, 2018.

[11] Liu, Tianliang, et al. "A cable-driven redundant spatial manipulator with improved stiffness and load capacity." 2018 IEEE/RSJ International Conference on Intelligent Robots and Systems (IROS). IEEE, 2018.

[12] Yang, Taiwei, et al. "Development of a cable-driven redundant space manipulator with large bending angle by combining quaternion joints and segmented coupled linkages mechanism." Chinese Journal of Aeronautics (in press).

[13] Hoyoung Kim, Hosu Lee, Jungwon Yoon. "Nematode-Inspired Cable Routing Method for Cable Driven Redundant Manipulator." 2023 IEEE/RSJ International Conference on Intelligent Robots and Systems (IROS). IEEE, 2023 (in press)

[14] Hickman, Cleveland P. Integrated principles of zoology. Michael D. Lange, 2021(18th ed, p.394)

[15] Bonev, Ilian A., and Jeha Ryu. "A new approach to orientation workspace analysis of 6-DOF parallel manipulators." Mechanism and machine theory 36.1 (2001): 15-28.

[16] Yuan, Han, et al. "Analytical and numerical methods for the stiffness modeling of cable-Driven serpentine manipulators." Mechanism and Machine Theory 156 (2021): 104179.

[17] Liu, Tianliang, et al. "A hybrid active and passive cable-driven segmented redundant manipulator: design, kinematics, and planning." IEEE/ASME Transactions on Mechatronics 26.2 (2020): 930-942.